

Itinerant and local-moment magnetism in EuCr_2As_2 single crystals

U. B. Paramanik,¹ R. Prasad,¹ C. Geibel,² and Z. Hossain^{1,2,*}

¹*Department of Physics, Indian Institute of Technology, Kanpur 208016, India*

²*Max-Planck Institute for Chemical Physics of Solids, 01187 Dresden, Germany*

(Dated: May 6, 2014)

We report on the crystal structure, physical properties and electronic structure calculations for the ternary pnictide compound EuCr_2As_2 . X-ray diffraction studies confirmed that EuCr_2As_2 crystallizes in the ThCr_2Si_2 -type tetragonal structure (space group I_4/mmm). The Eu-ions are in a stable divalent state in this compound. Eu moments in EuCr_2As_2 order magnetically below $T_m = 21$ K. A sharp increase in the magnetic susceptibility below T_m and the positive value of the paramagnetic Curie temperature obtained from the Curie-Weiss fit suggest dominant ferromagnetic interactions. The heat capacity exhibits a sharp λ -shape anomaly at T_m , confirming the bulk nature of the magnetic transition. The extracted magnetic entropy at the magnetic transition temperature is consistent with the theoretical value $R\ln(2S+1)$ for $S = 7/2$ of the Eu^{2+} ion. The temperature dependence of the electrical resistivity $\rho(T)$ shows metallic behavior along with an anomaly at 21 K. In addition, we observe a reasonably large negative magnetoresistance ($\sim -24\%$) at lower temperature. Electronic structure calculations for EuCr_2As_2 reveal a moderately high density of states of Cr-3d orbitals at the Fermi energy, indicating that the nonmagnetic state of Cr is unstable against magnetic order. Our density functional calculations for EuCr_2As_2 predict a G-type AFM order in the Cr sublattice. The electronic structure calculations suggest a weak interlayer coupling of the Eu-moments.

PACS numbers: 74.70.Xa, 75.50.Cc, 75.40.Cx, 71.20.-b

I. INTRODUCTION

The layered pnictide intermetallic compounds RT_2Pn_2 (R = rare-earth elements, T = transition metal; Pn = pnictide) with ThCr_2Si_2 -type tetragonal structure (space group I_4/mmm) exhibit a rich variety of transport and magnetic properties. These compounds consist of alternate ‘T-Pn’ layers and ‘R’ layers stacked along the c axis. Following the exploration of these materials over the last 20 years, recently, the discovery of high temperature superconductivity (SC) in the doped AFe_2As_2 (A = divalent alkaline metal or rare-earth metal) has generated a new wave of investigations in search of new compounds in this class, which exhibit interesting magnetic and superconducting properties. The Fe atoms in these materials undergo a spin-density-wave (SDW) antiferromagnetic (AFM) transition below 200 K. Upon doping or under application of external pressure, the Fe AFM ordering weakens and SC emerges.¹⁻⁵

Europium is among the few special rare-earth elements having two stable valence configurations: Eu^{2+} ($J = S = 7/2$) and Eu^{3+} ($J = 0$); Eu^{2+} bears a strong magnetic moment ($\sim 7.0 \mu_B$) whereas Eu^{3+} does not carry any moment. In a few cases a mixed-valence state of Eu is also observed, for example, in EuNi_2P_2 and EuCu_2Si_2 [6,7,8]. EuFe_2As_2 is a member of the Fe based ‘‘122’’ pnictide family where Eu is divalent. This system undergoes a SDW transition in the Fe sublattice at 190 K accompanied by an AFM ordering of Eu^{2+} moments at 19 K [9]. The interplay between SC and Eu^{2+} magnetism in doped EuFe_2As_2 has been extensively studied recently.^{4,5,9-12} Replacing As by P in EuFe_2P_2 , no Fe moment has been observed in the system and the divalent Eu moments

order ferromagnetically at $T_C = 30$ K as has been detected by neutron diffraction measurements.^{13,14} Incommensurate antiferromagnetic structure of Eu^{2+} moments with $T_N = 47$ K has been found in EuRh_2As_2 [15]. While EuCu_2As_2 exhibits a delicate balance between FM and AFM ordering,¹⁶ EuNi_2As_2 and EuCo_2As_2 order antiferromagnetically.^{17,18} Briefly, the pnictide compounds of this structure class show a variety of novel and interesting behaviors.

We synthesized a new isostructural compound, EuCr_2As_2 . This compound crystallizes in the ThCr_2Si_2 -type tetragonal structure with space group I_4/mmm . As shown in Fig. 1, alternating Eu layers and CrAs layers are stacked along the c axis where Cr atoms form a square planar lattice in the CrAs layer, similar to the AFe_2As_2 . Recently, Singh et al. have investigated the closely related compound BaCr_2As_2 [19]. A combined study of physical properties and electronic structure calculations demonstrate that BaCr_2As_2 is a metal with itinerant antiferromagnetism, similarly to the parent phases of Fe-based superconductors but with slightly different magnetic structure. Neutron diffraction measurements on $\text{BaFe}_{2-x}\text{Cr}_x\text{As}_2$ crystals reveal that the Cr doping in BaFe_2As_2 leads to suppression of the Fe SDW transition but the superconductivity (as usually observed in case of other transition metal doping) is prevented by a new competing magnetic order of G-type antiferromagnetism which becomes the dominant magnetic ground state for $x > 0.3$.^{20,21} BaCr_2As_2 shows stronger transition metal-pnictogen covalency than the Fe compounds,¹⁹ and in that respect is more similar to the widely studied compound BaMn_2As_2 . BaMn_2As_2 has been characterized as a small band-gap semiconductor with G-type AFM ordering of Mn moments at $T_N = 625$ K [22,23]. This ma-

terial becomes metallic by partial substitution of Ba by K or by applied pressure on the parent compound.^{24–26} In contrast to BaCr₂As₂ and BaMn₂As₂, both having tetragonal crystal structure, EuMn₂As₂ forms in hexagonal crystal structure²⁷ whereas EuCr₂As₂ is found to be tetragonal. Very recently, the closely related compounds LnOCrAs (Ln = La, Ce, Pr, and Nd) possessing similar CrAs layers as in BaCr₂As₂ have been synthesized by Park et al.²⁸ These compounds are isostructural (ZrCuSiAs-type structure with the space group $P4/nmm$) to that of LnOFeAs, which are the parent compounds of Fe-based high T_c superconductors. Powder neutron diffraction measurements at room temperature reveal that Cr²⁺ ions in LaOCrAs bear a large itinerant moment of $1.57 \mu_B$ pointing along the c axis which undergo a G-type AFM ordering. The Néel temperature T_N has been estimated to be in between 300-550 K. Therefore, the related materials possessing CrAs layers are highly enthralling with regard to the physical properties when the AFM ordering is suppressed by doping.

Here we report on the crystal structure, physical properties and electronic structure calculations of EuCr₂As₂. Our combined experimental investigations and density functional studies show that Eu-ions are in a divalent state and the Eu²⁺ local moments order magnetically at $T_m = 21$ K. $M(T)$ and $M(H)$ data suggest competing FM and AFM interactions since the $M(T)$ curves look like that of a ferromagnet while the $M(H)$ curves lack the features typically observed in a ferromagnet. A large negative magnetoresistance is found below T_m . Density-functional theory-based calculations indicate that the Cr ions bear itinerant moments and the most stable magnetic state in the Cr sublattice is a G-type AFM order.

II. METHODS

The single crystals of EuCr₂As₂ were grown using CrAs flux as described by Singh et al.¹⁹ The CrAs binary was presynthesized by reacting the mixture of Cr powder and As pieces at 300 °C for 10 h, and then at 600 °C for 30 h and finally at 900 °C for 24 h. A ratio of Eu : CrAs = 1 : 4 was placed in an alumina crucible, and sealed inside a tantalum tube. The assembly was put into a furnace and heated to 1230 °C slowly and held there for 13 hours, and then was cooled to 1120 °C at a rate of 2 °C/h, finally it was furnace-cooled to room temperature. The shiny plate-like EuCr₂As₂ crystals were formed in layers, which were cleaved mechanically from the flux. Several plate like single crystals with typical dimension $4 \times 4 \times 0.2$ mm³ were obtained. The polycrystalline samples of EuCr₂As₂ were prepared using solid state reaction method similar to that of EuFe₂As₂ as described in our earlier reports.^{4,9,11} Stoichiometric amounts of the starting elements of Eu chips (99.9%), Cr powder (99.999%), and As chips (99.999%) were used for the reaction. The single crystals and crushed polycrystalline samples were characterized by x-ray diffrac-

tion (XRD) with Cu- K_α radiation to determine the single phase nature and crystal structure. Scanning electron microscope (SEM) equipped with energy dispersive x-ray (EDX) analysis was used to check the homogeneity and composition of the samples. The electrical transport properties were measured by standard four probe technique using close cycle refrigerator (Oxford Instruments) and physical property measurement system (PPMS-Quantum design). The $\chi(T) = M(T)/H$ and $M(H)$ isotherms were measured using a commercial SQUID magnetometer (MPMS, Quantum-Design). The specific heat was measured by relaxation method in a PPMS-Quantum design.

We have carried out the density-functional band structure calculations using the full potential linear augmented plane wave plus local orbitals (FP-LAPW+lo) method as implemented in the WIEN2k code.²⁹ The Perdew-Burke-Ernzerhof (PBE) form of the generalized gradient approximation (GGA) was used to calculate the exchange correlation potential.³⁰ Additionally, to correct the on-site strong Coulomb interaction within the Eu-4*f* orbitals we have included U on a mean-field level using the GGA+U approximation. No spectroscopy data for EuCr₂As₂ are available in the literature, therefore, we have used U = 8 eV, the standard value for an Eu²⁺ ion.^{4,9,31} In addition, the spin orbit coupling is included with the second variational method in the Eu-4*f* shell. The set of plane-wave expansion K_{MAX} was determined as $R_{MT} \times K_{MAX}$ equals to 7.0 and the K -mesh used was $10 \times 10 \times 10$.

III. RESULTS AND DISCUSSION

A. Crystal Structure

Fig. 1 shows the powder XRD pattern at room temperature for the crushed polycrystalline sample of EuCr₂As₂. All the diffraction peaks could be indexed based on the ThCr₂Si₂-type structure (space group $I4/mmm$). The crystallographic lattice parameters are listed in Table I. The c/a ratio for EuCr₂As₂ is much larger than that of other Eu based transition metal pnictides. A comparison of the structural parameters is shown in Table III. An increased c/a ratio has also been observed in the homologous compound BaCr₂As₂ ($a = 3.96$ Å and $c = 13.632$ Å) [19] as compared to other transition metal compounds BaT₂As₂. The inset of Fig. 1 shows the x-ray diffraction pattern for a EuCr₂As₂ single crystal. Only the (001) diffraction peaks are observed, confirming that the crystallographic c axis is perpendicular to the plane of the plate-like single crystals. From the EDX analysis, the single phase nature of the sample is manifested with obtained atomic ratio of Eu : Cr : As as 20.8 : 38.3 : 40.9.

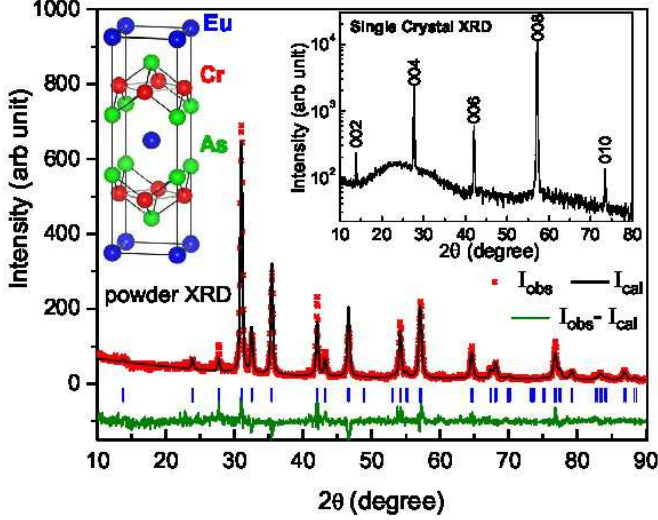


FIG. 1: (Color online) (a) The powder x-ray diffraction pattern of EuCr_2As_2 recorded at room temperature. The Rietveld refinement fit (solid black line), difference profile (lower solid green line) and positions of Bragg peaks (vertical blue bars) are also shown. Inset: x-ray diffraction pattern for EuCr_2As_2 plate-like single crystal.

TABLE I: Crystallographic parameters obtained from the structural Rietveld refinement of powder XRD data of EuCr_2As_2 . The refinement quality parameter $\chi^2 = 1.62$.

Structure		ThCr ₂ Si ₂ -type Tetragonal		
Space group		$I4/mmm$		
Lattice parameters				
a (Å)		3.893(2)		
c (Å)		12.872(2)		
V_{cell} (Å ³)		195.08(1)		
Refined Atomic Coordinates				
Atom	Wyckoff	x	y	z
Eu	2a	0	0	0
Cr	4d	0	0.5	0.25
As	4e	0	0	0.363

B. Magnetic susceptibility and isothermal magnetization

Fig. 2 shows the temperature dependence of the magnetic susceptibility $\chi_{ab}(T)$ for EuCr_2As_2 with the applied magnetic field $H = 1$ kOe along the crystallographic ab -plane ($H\parallel ab$). There is a sharp increase in $\chi_{ab}(T)$ below 21 K which tend to saturate at lower temperature as in the case of a ferromagnetic order. At high temperature $\chi_{ab}(T)$ follows the modified Curie-Weiss behavior, $\chi(T) = \chi_0 + C/(T - \theta_P)$ where χ_0 is the temperature-independent term of the susceptibility, C is the Curie constant and θ_P is the Weiss temperature. The fitting of inverse susceptibility data by the Curie-Weiss behavior in the temperature range 50-300 K (shown by the solid line) yields the effective paramagnetic moment $\mu_{eff} = 7.95 \mu_B$ and $\theta_P = 19$ K. Similar fit for $\chi_c(T)$ data (not

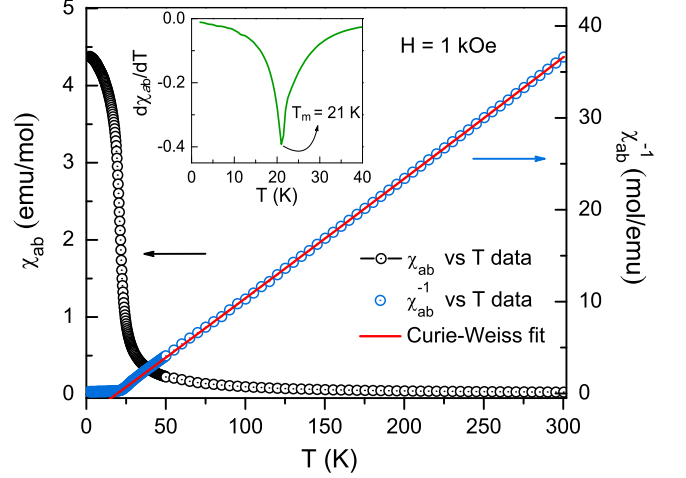


FIG. 2: (Color online) Temperature dependence of magnetic susceptibility χ_{ab} for EuCr_2As_2 with the applied magnetic field $H = 1$ kOe. The solid line represents the fit to the Curie-Weiss behavior.

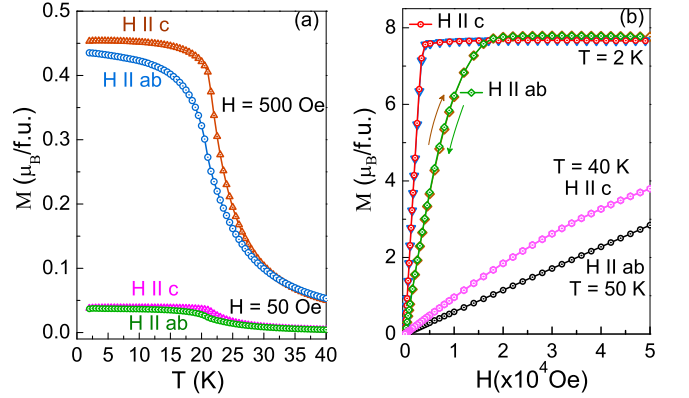


FIG. 3: (Color online) (a) Temperature dependence of magnetization M of EuCr_2As_2 single crystal under applied field of 50 Oe and 500 Oe with H in the ab plane ($H\parallel ab$) and parallel to the crystallographic c axis ($H\parallel c$). All the data shown are in zero field cooled (ZFC) condition. (b) Isothermal magnetization M of EuCr_2As_2 single crystal with $H\parallel ab$ and $H\parallel c$. M - H data were corrected for the demagnetization effect, taken on a plate-like sample.

shown here) yields the effective paramagnetic moment $\mu_{eff} = 8.27 \mu_B$ and $\theta_P = 22$ K. For both χ_{ab} and χ_c , the effective paramagnetic moments are close to the theoretical value of $g\sqrt{S(S+1)}\mu_B = 7.94 \mu_B$ for free Eu^{2+} moments ($S = 7/2$, $L = 0$). The positive values of the paramagnetic Curie temperature θ_P obtained from the fit suggest predominantly ferromagnetic exchange interactions between the Eu^{2+} moments.

Fig. 3(a) represents the magnetization $M(T)$ in two different orientations of magnetic field, i.e. $H\parallel ab$ and $H\parallel c$. At high temperature $M(T)$ is almost isotropic, as normally observed for a stable divalent Eu state. Since it bears a spin only ($J = S = 7/2$) moment, one ex-

pects a negligible anisotropy. However, a significant anisotropy in the magnetization is developed below 25 K ($M_{H\parallel c}/M_{H\parallel ab} \approx 1.5$ at 21 K), suggesting an anisotropic magnetic interaction. The rapid increase of $M(T)$ below 21 K gives an impression that the magnetic order is either ferromagnetic in nature or it has a strong ferromagnetic component. To gain further insight on the nature of the magnetic order we have carried out isothermal magnetization measurements with varying magnetic fields at fixed temperatures [Fig. 3(b)]. At temperature $T = 2$ K, the magnetization for $H\parallel c$ saturates more rapidly as the magnetic field is increased from $H = 0$ to 4.1 kOe. For $H\parallel ab$, the magnetization saturates at much higher field (18 kOe). A sizable magnetic field is required to achieve the saturation of magnetization for both $H\parallel ab$ and $H\parallel c$. We do not observe any hysteresis in the $M(H)$ curve at 2 K. It is known that a good quality single crystal of a ferromagnet with small anisotropy and thus small domain wall energy may not always exhibit remanent magnetization.³² Thus, one cannot rule out the possibility of a FM state of Eu^{2+} moments in EuCr_2As_2 . However, combining the experimental results with the electronic structure calculations (to be discussed below) where we get an antiferromagnetic ground state of the interlayer Eu moments with very weak interlayer coupling, it is possible that the dominant nearest-neighbor (i.e. intralayer) Eu-Eu interaction is FM as indicated by a positive value of θ_P , but there could be a weak or frustrated AFM coupling between the layers. In this connection, we may recall other homologous compounds EuCu_2As_2 or EuFe_2As_2 , wherein the intralayer Eu-Eu interaction has been established to be ferromagnetic, while the interlayer antiferromagnetic coupling is very weak.^{16,33-35} If we consider the interlayer Eu-Eu antiferromagnetic coupling to be very weak in EuCr_2As_2 , then, a small external magnetic field as employed in our magnetic measurements can reorient the spin arrangement along the field direction at the onset of magnetic ordering. The saturated magnetization at 2 K is determined to be $\sim 7.78 \mu_B/\text{f.u.}$ and $\sim 7.66 \mu_B/\text{f.u.}$ for $H\parallel ab$ and $H\parallel c$ respectively, implying that the system is nearly isotropic. The measured saturated magnetization for both the directions are more than that expected for parallelly aligned Eu^{2+} moments ($gS = 7.0 \mu_B/\text{f.u.}$ with $g = 2$, $S = 7/2$), indicating that the Cr ions carry an itinerant moment and are contributing to the total magnetization. The electronic structure calculations on EuCr_2As_2 (to be discussed below) also suggest that Cr carries an itinerant moment and the most stable magnetic structure in the Cr sublattice is a G-type AFM order. The homologous compound BaCr_2As_2 has been proposed to be a metal with itinerant antiferromagnetism.¹⁹ In fact, neutron diffraction measurements on $\text{BaFe}_{2-x}\text{Cr}_x\text{As}_2$ crystals reveal that for $x > 0.3$, the magnetic ground state is consistent with G-type AFM order.²¹ It also suggests that the Cr magnetic ordering could be well above room temperature in the BaCr_2As_2 parent compound similar to BaMn_2As_2 [23] which also exhibits a G-type AFM ordering of Mn

moments at $T_N = 625$ K. Moreover, the closely related compounds LnOCrAs s possessing similar CrAs layers, in which, Cr ions bear a large itinerant moment of $1.57 \mu_B$ and undergo a G-type AFM ordering with Néel temperature in between 300–550 K.²⁸ Similar magnetic ordering of Cr in EuCr_2As_2 is also possible at higher temperature.

C. Specific heat

Fig. 4 shows the plots of temperature dependence of heat capacity $C_P(T)$ of the EuCr_2As_2 single-crystal and that of the reference compound BaCr_2As_2 taken from ref. 19. The $C_P(T)$ of EuCr_2As_2 exhibits a sharp λ -type anomaly due to the magnetic transition at $T_m = 21$ K, indicating that the magnetic transition is of second-order. The anomaly in $C_P(T)$ remains undisturbed under applied field of 500 Oe but with increasing field up to 5 kOe the anomaly is reduced significantly in height and considerably broadened suggesting a field induced change of the nature of the magnetic transition, presumably a field stabilized ferromagnetic order. The magnetic anomaly in the $C_P(T)$ makes it difficult to fit the data at lower temperature to extract the electronic specific-heat coefficient (γ). The measured value of $C_P(T)/T$ at 2 K is ≈ 225 mJ/molK², but the estimation of γ from this value is not reliable as there are magnon contribution from the nearby magnetic ordering of Eu moments. A large $C_P(T)/T$ (≈ 250 mJ/molK²) at 2 K was also observed in ferromagnetically ordered EuFe_2P_2 [13].

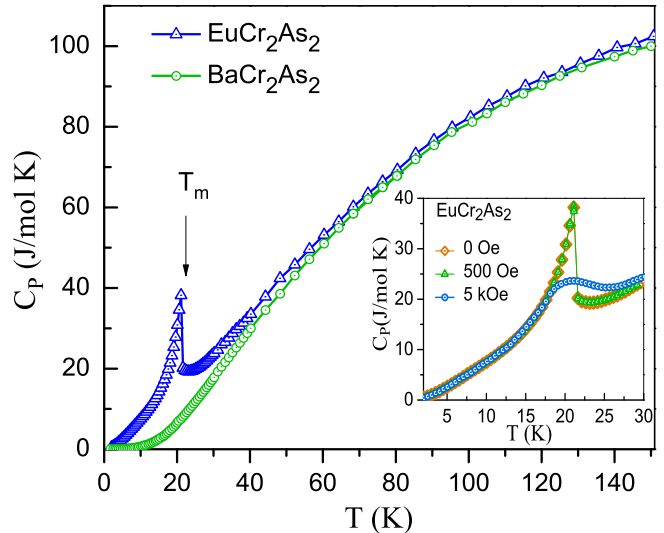


FIG. 4: (Color online) Temperature dependence of the specific heat C_P of EuCr_2As_2 single crystal and that of the reference compound BaCr_2As_2 taken from ref. 19. The lower inset shows the C_P of EuCr_2As_2 at zero field and under external fields of 500 Oe and 5 kOe.

The magnetic part of heat capacity $C_{mag}(T)$ was deduced by the usual method of subtracting the heat capacity of BaCr_2As_2 from that of EuCr_2As_2 after adjust-

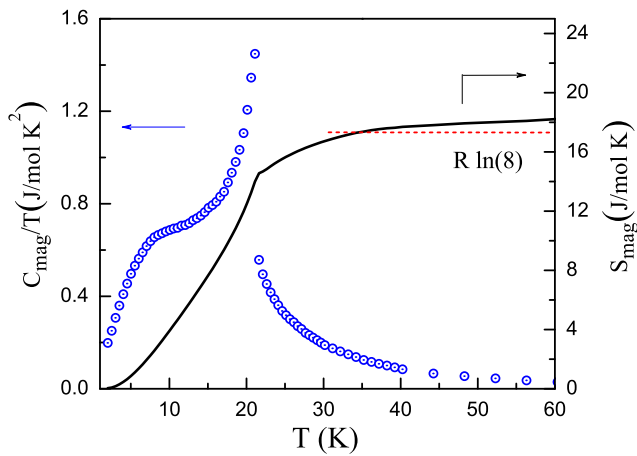


FIG. 5: (Color online) C_{mag}/T vs T of EuCr_2As_2 and the calculated magnetic entropy S_{mag} vs T shown by the solid line.

ing the renormalization due to different atomic masses of Ba and Eu, although the mass difference is small here. Based on the mean-field theory,³⁶ the heat-capacity jump at the magnetic transition is calculated for the two possible magnetic structures: (i) the equal moment (EM) structure where the magnetic moments are the same at all sites and (ii) the amplitude modulated (AM) structure where the magnetic-moment amplitude varies periodically from one site to another. For EM structure, the jump in the heat capacity at the ordering temperature is given by³⁶

$$\Delta C_{EM} = 5 \frac{J(J+1)}{(2J^2 + 2J + 1)} R \quad (1)$$

and for AM structure,

$$\Delta C_{AM} = \frac{10}{3} \frac{J(J+1)}{(2J^2 + 2J + 1)} R \quad (2)$$

where J is the total angular momentum and R is the gas constant. By using $J = S = 7/2$ for divalent Eu, ΔC_{EM} and ΔC_{AM} amounts to 20.15 J/molK and 13.4 J/molK respectively. Our estimated ΔC (≈ 20.25 J/molK) at T_m suggests that EuCr_2As_2 possesses an EM structure. In addition, a hump appears in the specific heat at $T \sim T_m/3$, which arises naturally within the mean-field theory for a $(2J+1)$ -fold degenerate multiplet. The hump is seen in experimental $C_{mag}(T)$ for EuCr_2As_2 , which is more pronounced in the C_{mag}/T versus T plot (Fig. 5). The hump in the ordered state is particularly noticeable in compounds containing Eu^{2+} or Gd^{3+} with $S = 7/2$, and is not visible for lower S , e.g., $S = 1/2$ [36, 37, 38]. The magnetic contribution to the entropy S_{mag} was obtained by integrating the C_{mag}/T versus T . The C_{mag}/T data were extrapolated from $T = 2$ K to $T = 0$ in order to approximate the missing C_{mag}/T data between 0 and 2 K. As can be seen from Fig. 5, the S_{mag} saturates to the expected theoretical value $R \ln(2S + 1) =$

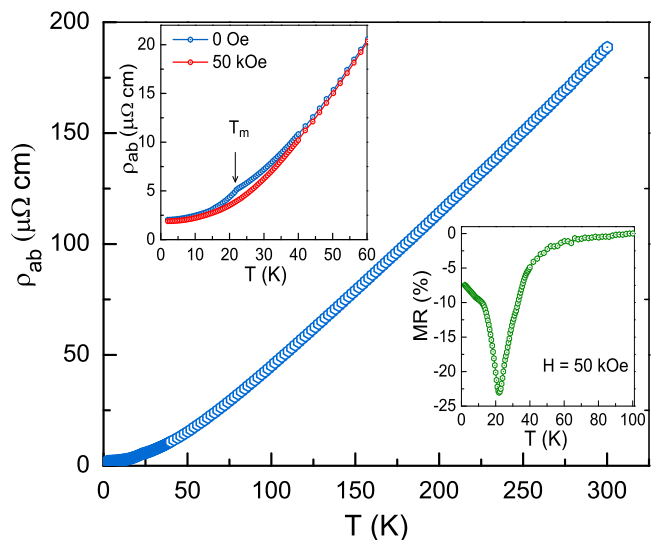


FIG. 6: (Color online) Temperature dependence of in plane resistivity ρ_{ab} for EuCr_2As_2 under zero applied magnetic field. The upper inset shows an enlarge view of ρ_{ab} under applied magnetic fields of 0 and 50 kOe parallel to the c -axis. The lower inset shows the temperature dependence of magnetoresistance for EuCr_2As_2 .

17.3 J/molK, where $S = 7/2$ for Eu^{2+} . The magnetic entropy $S_{mag} = 14.6$ J/molK at T_m is 84% of the theoretical value.

D. Transport Properties

The temperature dependence of in-plane electrical resistivity $\rho_{ab}(T)$ of EuCr_2As_2 as shown in Fig. 6 exhibits a metallic behavior with residual resistivity $\rho_{ab} = 2.0$ $\mu\Omega$ cm at 2 K and residual resistivity ratio (RRR) = $\rho_{300\text{K}}/\rho_{2\text{K}} \approx 90$. The high residual resistivity ratio together with a low residual resistivity confirms the high quality of our crystals. Since the compound is metallic, most likely the magnetic coupling between the Eu spins is mainly mediated by the conduction electrons through indirect Ruderman-Kittel-Kasuya-Yosida (RKKY) interaction. The resistivity data show a kink at the magnetic transition temperature (T_m) followed by a rapid decrease in resistivity below T_m due to reduction of spin disorder scattering. Further, we observe significant reduction of the electrical resistivity adjacent to the magnetic ordering temperature on application of magnetic field, leading to a negative magnetoresistance (MR). The MR reaches its maximum value (-24%) near T_m . The MR [Fig. 6] is defined as $[\rho(H) - \rho(0)]/\rho(0)$, where $\rho(0)$ and $\rho(H)$ are the resistivity measured at zero field and under applied field $H = 50$ kOe respectively.

E. Density-functional calculations

In order to study the electronic and magnetic properties of the compound we start with the calculation of the density of states (DOS) for EuCr_2As_2 in the quenched paramagnetic state, that means no spin polarization is allowed on the Cr ions, but, spin polarization is enabled for the Eu ions. Such a study can provide an intimation of magnetic state for the transition metal ions by analyzing the partial density of states (PDOS) at the Fermi level and we can infer whether the magnetic state is favored or not. A similar approach was adopted in prior calculations for EuFe_2As_2 [12, 31] and the DOS of which is shown here for comparison purposes. We use the experimental lattice parameters $a = 3.893(2)$ Å, and $c = 12.872(2)$ Å of EuCr_2As_2 for the calculations. The internal coordinate of As ($z_{\text{As}} = 0.361$) is determined by force minimization, which is very close to the experimental z_{As} for EuCr_2As_2 . For the reference compound EuFe_2As_2 , the experimental lattice parameters were taken from ref. 9.

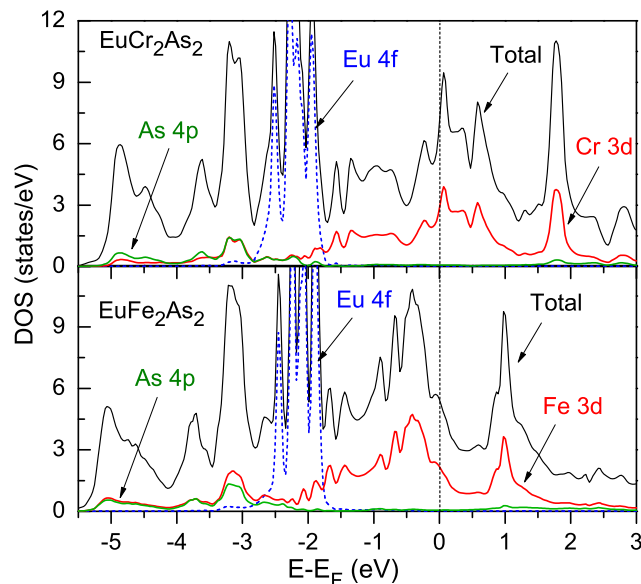


FIG. 7: (Color online) Total and partial Densities of states (DOS) for EuCr_2As_2 and EuFe_2As_2 in the NM state in Cr/Fe sublattice and FM interaction between the intralayer Eu spins in the Eu sublattice.

The general shape of our density of states for EuCr_2As_2 (Fig. 7) is similar to that for EuFe_2As_2 , but, with a shift of 3d orbitals in the binding energy, which is expected as Cr has two 3d electrons less as compared to Fe. The calculated DOS for EuFe_2As_2 is very similar to that reported by Li et al.³¹ The Eu 4f states for both the compounds are quite localized in between -1.5 to -3 eV, suggesting that the Eu ions are in a stable 2+ valence state. The calculated spin moment for Eu^{2+} is about $6.9 \mu_B$ which is consistent with the experimental value. The rest of the DOS can be divided into two parts: (i) The DOS below -2 eV consists of hybridized Cr 3d and As 4p

TABLE II: Results of Energetic and magnetic properties of EuCr_2As_2 for different magnetic states in the Cr sublattice and interlayer AFM coupling in the Eu sublattice. ΔE (eV) is the total energy difference per formula unit basis (two Cr atoms) with respect to the non-spin-polarize or non-magnetic state, and $m_{\text{Cr}}(\mu_B)/m_{\text{Eu}}(\mu_B)$ is the calculated magnetic moment on Cr/Eu. (NM = non-magnetic or non-spin-polarized, FM = ferromagnetic, S-AFM = stripe type AFM order, G-AFM = G-type AFM or checkerboard nearest-neighbor AFM order).

Cr-ordering	ΔE (eV)	$m_{\text{Cr}}(\mu_B)/m_{\text{Eu}}(\mu_B)$
NM	0	0/6.9
FM	-0.136	1.28/6.9
S-AFM	-0.064	1.69/6.9
G-AFM	-0.417	2.10/6.9

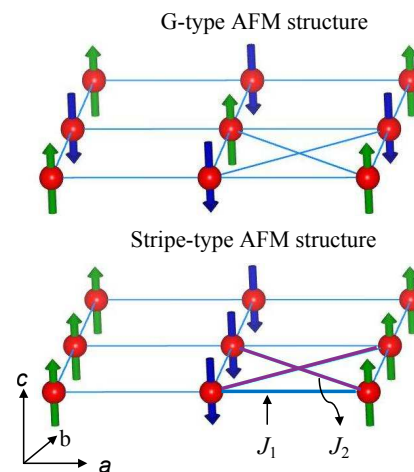


FIG. 8: (Color online) The top panel shows the G-type (Néel or checkerboard) AFM structure where nearest-neighbor spins are aligned antiparallel. The bottom panel represents stripe-type AFM ordering along with the definitions of the in-plane exchange constants J_1 and J_2 .

orbitals. The p - d hybridization between As 4p and Cr 3d is sizable. (ii) The DOS near the Fermi level ranging from -2 eV to +2 eV is basically composed of the Cr 3d orbitals. The Fermi level lies on a steep edge of a peak in the partial density of states of Cr-3d orbitals, resulting in a relatively large DOS at the Fermi energy. The corresponding value of PDOS at the Fermi level for Cr-3d is $N(E_F) = 3.03$ states/eV per Cr atom, which is greater than that of Fe-3d states (2.15 states/eV per Fe atom) in EuFe_2As_2 [31]. According to the Stoner criterion, magnetism may occur if $N(E_F) * I > 1$, where I is the Stoner exchange-correlation integral.³⁹ We use the Stoner exchange-correlation integral $I = 0.38$ eV for Cr-3d from the original work of Janak,⁴⁰ which amounts to $N(E_F) * I = 1.15$. Therefore, the non magnetic (NM) state of Cr is unstable against the magnetic order in EuCr_2As_2 .

TABLE III: A comparison of the structural and magnetic parameters of EuCr_2As_2 with some isostructural Eu compounds. The lattice parameters a and c are at room temperature, T_N/T_C are the antiferromagnetic/ferromagnetic ordering temperatures and μ_{eff} is the effective moment calculated from the Curie-Weiss fit of magnetic susceptibility data.

Compound	$a(\text{\AA})$	$c(\text{\AA})$	$T_N/T_C(K)$	$\mu_{eff}(\mu_B/\text{f.u.})$	Ref.
EuFe_2As_2	3.907	12.114	19	7.79	9
EuCu_2As_2	4.260	10.203	15	7.90	16
EuNi_2As_2	4.096	10.029	14	7.30	17,42
EuCo_2As_2	3.934	11.511	39	7.40	18,42
EuCr_2As_2	3.893	12.872	21	7.95	This work

To examine the most stable magnetic structure of Cr in EuCr_2As_2 , we have calculated the total energy for different possible magnetic states, namely, (i) a non-spin polarized calculation (no magnetism on Cr), (ii) FM spin configuration, (iii) stripe-type AFM (similar to that in EuFe_2As_2) and (iv) G-type AFM. The corresponding total energies of different magnetic states together with the calculated moment values are listed in Table II. It is shown that a G-type AFM order in the Cr sublattice is the lowest energy state for EuCr_2As_2 . The large energy differences between different Cr magnetic configurations suggest that the magnetic ordering temperature of Cr moments should be high. BaCr_2As_2 also possess a G-type AFM ground state of Cr itinerant moments as has been reported by Singh et al.¹⁹ Neutron diffraction studies on $\text{BaFe}_{2-x}\text{Cr}_x\text{As}_2$ show a G-type AFM ground state for $x > 0.3$ [21]. Recent experimental investigation on the closely related compound LaOCrAs reveal a G-type AFM order of Cr itinerant moments of $1.57 \mu_B$ [28]. Therefore, our calculation of minimum ground state energy for a G-type AFM order of Cr moments in EuCr_2As_2 agrees with the magnetic structure of other related compounds. According to the Heisenberg model with nearest-neighbor (J_1) and next-nearest-neighbor (J_2) spin interactions, the differences in the ordered energies for several collinear commensurate magnetic structures are given by⁴¹

$$E_{FM} - E_{G-AFM} = 2NS^2(2J_1) \quad (3)$$

and

$$E_{G-AFM} - E_{S-AFM} = 2NS^2(2J_2 - J_1) \quad (4)$$

where N is the number of spins S . The in-plane G-type AFM is favored when $J_1 > 0$ and $J_1 > 2J_2$. Our calculations yield an antiferromagnetic J_1 (> 0) and a large negative J_2 with $J_2/J_1 = -0.77$. The large negative value of J_2 implies that this model is probably not reliable for the system. This might be expected in a itinerant magnetic system with long range magnetic order, as has been pointed out by Singh et al. for the BaCr_2As_2 system.¹⁹

Experimentally we do not observe any signature of Cr moment ordering up to 300 K. This is not surprising considering the large total energy differences between different magnetic Cr moment configurations, which suggest

an ordering temperature well above the maximum temperature of our measurements. Magnetic measurements at higher temperature are needed to corroborate the expected AFM ordering of Cr moments. The calculated magnetic structure of Cr moments can be verified experimentally using neutron or x-ray scattering measurements.

Finally, we discuss the magnetic order in the Eu sublattice. The calculated total energy for the system is found to be minimum when the interlayer Eu spins are antiferromagnetically coupled. Nevertheless, the difference in total energy is very small (~ 0.0006 eV) whether the interlayer Eu spins are antiferromagnetically coupled or ferromagnetically coupled, implying a rather weak interlayer coupling in the Eu sublattice. So, it is expected that any small external effect (doping, external pressure or external magnetic field) can easily flip the Eu spin from AFM to FM. The P doped EuFe_2As_2 system witnesses a similar weak interlayer coupling (0-6 meV), wherein the antiferromagnetic Eu moments arrangement changes from AFM to FM with slight change in doping concentration.³³ Furthermore, the homologous system EuFe_2As_2 with antiferromagnetic ground state experiences a field-induced spin reorientation to the FM state for an applied field of just 1 T in the ab -plane and at 2 T along the c -axis,^{34,35} which suggests a weak AFM coupling between the interlayer Eu spins. Taking into consideration the relatively large interlayer distance between the Eu layers along the c axis (6.44 \AA for EuCr_2As_2 , and 6.057 \AA for EuFe_2As_2), the interlayer coupling of Eu spins in EuCr_2As_2 is expected to be even lesser.

IV. CONCLUSIONS

In summary, we have successfully synthesized single and poly crystals of EuCr_2As_2 and characterized them using x-ray diffraction, electrical resistivity $\rho(T)$, magnetization and specific heat $C_p(T)$ measurements. The powder XRD data confirm that this compound crystallizes in the body-centered tetragonal structure (space group I_4/mmm). The $C_p(T)$ and $\rho(T)$ data show anomalies at a temperature $T_m = 21$ K. While the susceptibility behavior apparently indicates a ferromagnetic order be-

low 21 K, the magnetization data in the ordered state do not show any hysteresis or spontaneous magnetization. Furthermore, the value of θ_P obtained from the Curie-Weiss fit in the paramagnetic state is positive and very close to the magnetic transition temperature. These observations indicate that the dominant nearest-neighbor (i.e. intralayer) Eu-Eu interaction is FM but there could be a weak or frustrated AFM coupling between the layers. Also, we do not rule out the possibility of a FM state of Eu^{2+} moments in EuCr_2As_2 . The measured saturated magnetization for both $H\parallel ab$ and $H\parallel c$ are larger than the theoretical value of $gS = 7.0 \mu_B$ per Eu atom, suggesting that the Cr moments possibly contribute to the observed saturated magnetization values. The $\rho(T)$ data confirm the metallic state of EuCr_2As_2 with a negative magnetoresistance (-24%) around the magnetic transition. The magnetic entropy $S_{mag}(T)$ at T_m is 84% of the theoretical value $R\ln(2S + 1)$ for $S = 7/2$ of the Eu^{2+} ion and the remaining 16% is recovered by ≈ 34 K. The electronic structure calculations indicate that the Cr ions carry itin-

erant moment and the most stable magnetic structure in the Cr sublattice is a G-type AFM order. Moreover, the large total energy differences between different magnetic Cr moment configurations suggest an ordering temperature well above the maximum temperature of our measurements. Higher temperature magnetic measurements are needed to observe the expected Cr moment ordering. Density-functional calculations suggest a very weak interlayer coupling between the Eu moments. It would be useful and interesting to determine the magnetic structures of EuCr_2As_2 by magnetic neutron or x-ray scattering measurements.

ACKNOWLEDGEMENTS

This work has been partially supported by the Council of Scientific and Industrial Research, New Delhi (Grant No. 80(0080)/12/ EMR-II).

-
- * Electronic address: zakir@iitk.ac.in
- ¹ M. Rotter, M. Tegel, and D. Johrendt, Phys. Rev. Lett. **101** 107006 (2008).
 - ² Kalyan Sasmal, Bing Lv, Bernd Lorenz, Arnold M. Guloy, Feng Chen, Yu-Yi Xue, and Ching-Wu Chu, Phys. Rev. Lett. **101** 107007 (2008).
 - ³ Athena S. Sefat, Rongying Jin, Michael A. McGuire, Brian C. Sales, David J. Singh, and David Mandrus, Phys. Rev. Lett. **101** 117004 (2008).
 - ⁴ H. S. Jeevan, Z. Hossain, Deepa Kasinathan, H. Rosner, C. Geibel, and P. Gegenwart, Phys. Rev. B **78**, 092406 (2008).
 - ⁵ C. F. Miclea, M. Nicklas, H. S. Jeevan, D. Kasinathan, Z. Hossain, H. Rosner, P. Gegenwart, C. Geibel, and F. Steglich, Phys. Rev. B **79**, 212509 (2009).
 - ⁶ R. Nagarajan, G. K. Shenoy, L. C. Gupta and E. V. Sampathkumaran, Phys. Rev. B **32**, 2846 (1985).
 - ⁷ Yuichi HIRANAKA, AiNAKAMURA, Masato HEDO, Tetsuya TAKEUCHI, Akinobu MORI, Yusuke HIROSE, Katsuya MITAMURA, Kiyohiro SUGIYAMA, Masayuki HAGIWARA, Takao NAKAMA, and Yoshichika ŌNUKI, Journal of the Physical Society of Japan **82**, 083708 (2013).
 - ⁸ B. C. Sales, and R. Viswanathan, J. Low. Temp. Phys. **23** 449 (1976).
 - ⁹ H. S. Jeevan, Z. Hossain, Deepa Kasinathan, H. Rosner, C. Geibel, and P. Gegenwart, Phys. Rev. B **78**, 052502 (2008).
 - ¹⁰ S. Zapf, D. Wu, L. Bogani, H. S. Jeevan, P. Gegenwart, and M. Dressel, Phys. Rev. B **84** 140503(R) (2011).
 - ¹¹ Anupam, V. K. Anand, P. L. Paulose, S. Ramakrishnan, C. Geibel, and Z. Hossain, Phys. Rev. B **85**, 144513 (2012).
 - ¹² U. B. Paramanik, Debarchan Das, R. Prasad, and Z. Hossain, J. Phys.: Condens. Matter **25**, 265701 (2013).
 - ¹³ Chunmu Feng, Zhi Ren, Shenggao Xu, Shuai Jiang, Zhu'an Xu, I. Nowik, I. Felner, Guanghan Cao, Kazuyuki Matsumabayashi and Yoshiya Uwatoko, Phys. Rev. B **82**, 094426 (2010).
 - ¹⁴ D. H. Ryan, J. M. Cadogan, Shenggao Xu, Zhu'an Xu, and Guanghan Cao, Phys. Rev. B **83**, 132403 (2011).
 - ¹⁵ Yogesh Singh, Y. Lee, B. N. Harmon, and D. C. Johnston, Phys. Rev. B **79** 220401(R) (2009).
 - ¹⁶ Kausik Sengupta, P. L. Paulose, E. V. Sampathkumaran, Th. Doert, and J. P. F. Jemietio, Phys. Rev. B **72** 184424 (2005).
 - ¹⁷ E. D. Bauer, F. Ronning, B. L. Scott, and J. D. Thompson, Phys. Rev. B **78** 172504 (2008).
 - ¹⁸ Jared Ballinger, Lowell E. Wenger, Yogesh K. Vohra, and Athena S. Sefat, J. App. Phys. **111** 07E106 (2012).
 - ¹⁹ D. J. Singh, A. S. Sefat, M. A. McGuire, B. C. Sales, and D. Mandrus, L. H. VanBebber, and V. Keppens, Phys. Rev. B **79**, 094429 (2009).
 - ²⁰ Athena S. Sefat, David J. Singh, Lindsay H. VanBebber, Yuriy Mozharivskiy, Michael A. McGuire, Rongying Jin, Brian C. Sales, Veerle Keppens, and David Mandrus, Phys. Rev. B **79**, 224524 (2009).
 - ²¹ K. Marty, A. D. Christianson, C. H. Wang, M. Matsuda, H. Cao, L. H. VanBebber, J. L. Zarestky, D. J. Singh, A. S. Sefat, and M. D. Lumsden, Phys. Rev. B **83**, 060509(R) (2011).
 - ²² Yogesh Singh, A. Ellern, and D. C. Johnston, Phys. Rev. B **79**, 094519 (2009).
 - ²³ Yogesh Singh, M. A. Green, Q. Huang, A. Kreyssig, R. J. McQueeney, D. C. Johnston, and A. I. Goldman, Phys. Rev. B **80**, 100403(R) (2009).
 - ²⁴ Abhishek Pandey, R. S. Dhaka, J. Lamsal, Y. Lee, V. K. Anand, A. Kreyssig, T. W. Heitmann, R. J. McQueeney, A. I. Goldman, B. N. Harmon, A. Kaminski, and D. C. Johnston, Phys. Rev. Lett. **108** 087005 (2012).
 - ²⁵ A. T. Satya, Awadhesh Mani, A. Arulraj, N. V. Chandra Shekar, K. Vinod, C. S. Sundar, and A. Bharathi, Phys. Rev. B **84**, 180515(R) (2011).
 - ²⁶ Abhishek Pandey, B. G. Ueland, S. Yeninas, A. Kreyssig, A. Sapkota, Yang Zhao, J. S. Helton, J. W. Lynn, R. J. McQueeney, Y. Furukawa, A. I. Goldman, and D. C. Johnston, Phys. Rev. Lett. **111** 047001 (2013).
 - ²⁷ R. Ruehl, W. Jeitschko, Mater. Res. Bull. **14**, 513 (1979).

- ²⁸ Sang-Won Park, Hiroshi Mizoguchi, Katsuaki Kodama, Shin-ichi Shamoto, Toshiya Otomo, Satoru Matsuiishi, Toshio Kamiya, and Hideo Hosono, *Inorg. Chem.* **52**, 13363 (2013)
- ²⁹ P. Blaha, K. Schwarz, G. K. H. Madsen, D. Kvasnicka, and J. Luitz, WIEN2k, An Augmented Plane Wave Plus Local Orbitals Program for Calculating Crystal Properties. Vienna University of Technology, Vienna (2001).
- ³⁰ J. P. Perdew, K. Burke, and M. Ernzerhof, *Phys. Rev. Lett.* **77**, 3865 (1996).
- ³¹ Wei Li, Jian-Xin Zhu, Yan Chen, and C. S. Ting, *Phys. Rev. B* **86**, 155119 (2012).
- ³² D. Givord, H. S. Li, R. Perrier de la Bâthie, *Solid State Commun.* **51**, 857 (1984).
- ³³ H. S. Jeevan, Deepa Kasinathan, Helge Rosner, and Philipp Gegenwart, *Phys. Rev. B* **83**, 054511 (2011).
- ³⁴ Shuai Jiang, Yongkang Luo, Zhi Ren, Zengwei Zhu, Cao Wang, Xiangfan Xu, Qian Tao, Guanghan Cao and Zhu'an Xu, *New J. Phys.* **11** 025007 (2009).
- ³⁵ Y. Xiao, Y. Su, W. Schmidt, K. Schmalzl, C. M. N. Kumar, S. Price, T. Chatterji, R. Mittal, L. J. Chang, S. Nandi, N. Kumar, S. K. Dhar, A. Thamizhavel, and Th. Brueckel, *Phys. Rev. B* **81**, 220406(R) (2010).
- ³⁶ J. A. Blanco, D. Gignoux, and D. Schmitt, *Phys. Rev. B* **43**, 13145 (1991).
- ³⁷ D. C. Johnston, R. J. McQueeney, B. Lake, A. Honecker, M. E. Zhitomirsky, R. Nath, Y. Furukawa, V. P. Antropov, and Y. Singh, *Phys. Rev. B* **84**, 094445 (2011).
- ³⁸ R. J. Goetsch, V. K. Anand, and D. C. Johnston, *Phys. Rev. B* **87**, 064406 (2013).
- ³⁹ D. J. Singh, *Phys. Rev. B* **78**, 094511 (2008).
- ⁴⁰ J. F. Janak, *Phys. Rev. B* **16**, 255 (1977).
- ⁴¹ David C. Johnston, *Advances in Physics* **59**, 803 (2010).
- ⁴² H Raffius, E Mörsen, B.D Mosel, W Müller-Warmuth, W Jeitschko, L Terbüchte, and T Vomhof, *J. Phys. Chem. solid* **54**, 135 (1993).